Competition between deflection and penetration at an interface in the vicinity of a main crack

Eric Martin, Benoît Poitou, Dominique Leguillon, Jean Marie Gatt

Competition between deflection and penetration at an interface in the vicinity of a main crack

E. Martin, **B. Poitou**, **D. Leguillon**, **J. M. Gatt**

Abstract The mechanisms which govern crack deflection and crack penetration at interfaces must be understood in order to design composites and layered materials. Experimental observations have shown that a realistic description of crack deflection must take into account the initiation of fracture mechanisms by the stress field of an approaching matrix crack. Fracture mechanisms which include interfacial debonding and penetration are thus analysed in the vicinity of a main crack. For this purpose, a unit cell consisting of a single fibre surrounded by a cylindrical tube of matrix is studied with the help of a finite element model. Initiation stress and nucleation length are determined for both mechanisms by using an initiation criterion which requires to fulfil an energy and a stress condition. Investigating the competition between the initiation of the two mechanisms provides decohesion/penetra-tion maps which depend on the strength and toughness of interface and fibre. It is shown that the debonding or penetration condition can be reduced to an energy or a stress condition depending on the relative value of some characteristic fracture lengths of interface and fibre. Finally it is noted that a low toughness interface is not systematically a sufficient condition to promote the initiation of deflection.

Keywords Crack initiation · Interfacial fracture mechanics · Composite materials

1 Introduction

Increasing the reliability of brittle composites or laminated systems requires to control interfacial crack deflection. Ceramic matrix composites demonstrate damage tolerance if

E. Martin (✉) · B. Poitou
LCTS, CNRS UMR 5801, Université Bordeaux 1, Pessac, France
e-mail: martin@lcts.u-bordeaux1.fr

B. Poitou · J. M. Gatt
CEA, Cadarache DEN/CAD/DEC/SESC, St Paul lez Durance, France

D. Leguillon
LMM, CNRS UMR 7607, Université P. et M. Curie, Paris, France

matrix cracks are deflected along the fibre/matrix interfaces (Evans et al. 1991). Laminated ceramic materials offer substantial toughening as a result of the promotion of interfacial cracking under flexural loading (Phillipps et al. 1994). In both cases, improved toughness compared to monolithic ceramics is obtained as a consequence of the mechanism of crack deflection at an interface which must be understood to design the adequate interface (Kerans et al. 2002). Detailed fracture observations are difficult but various studies in brittle matrix composites have shown that the interface separates before the arrival of the matrix crack at the fibre (Majumdar et al. 1998; Pagano 1998). This mechanism was also observed in model laminates and bimaterials as shown by (Lee et al. 1996; Kagawa and Goto 1998; Xu et al. 2003). Those experimental observations indicate that a realistic description of crack deflection must take into account the initiation of fracture mechanisms by the stress field of an approaching crack.

As illustrated by Fig. 1, the aim of this paper is to analyse the initiation of interfacial debonding and penetration in the vicinity of a main crack. After crack onset, it is assumed that the main crack will join the initiated secondary crack. Analysing the competition between the two mechanisms will thus provide the capability of the interface to promote crack deflection. This approach is different from previous studies which focus on the competition between crack penetration and crack deflection with the crack tip located at the bimaterial interface (He and Hutchinson 1989; Martinez and Gupta 1994; Martin et al. 2001; Parmigiani and Thouless 2006). Previous authors (Leguillon et al. 2000; Martin and Leguillon 2004) have attempted to describe the initiation of interfacial debonding in the vicinity of a main crack with the help of an energy analysis but this approach does not always allow to evaluate the initiation stress and the corresponding nucleation length. In the present work, use is made of a more adequate criterion which combines an energy and a stress conditions. The competition between the two fracture mechanisms can be analysed in order to elucidate the roles of the

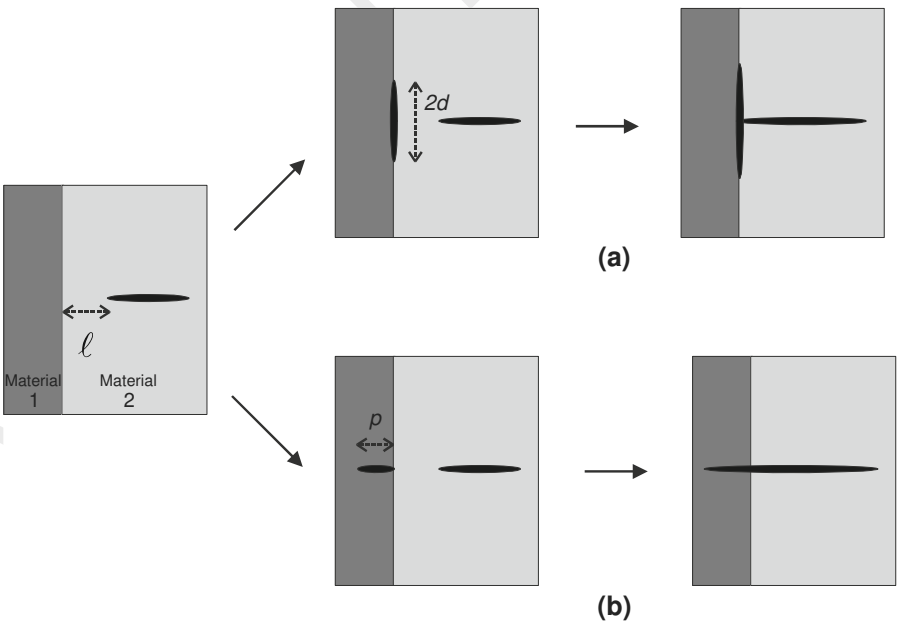

Fig. 1 A stationary main crack located near an interface: (**a**) nucleation of a debonding crack of length 2*d* and crack deflection at the interface and (**b**) nucleation of a penetrating crack of length *p* and crack penetration into the interface

strength and toughness of the components (including the interface) of the bimaterial on crack deflection. The studied geometry is a composite cell made of a single fibre embedded in a cylinder of matrix. It is assumed to be representative of a composite system but the results are presented in non-dimensional terms to evidence the dominating parameters which are expected to be qualitatively similar for laminated geometries.

2 The initiation criterion

Crack initiation in brittle elastic materials is usually based on stress distribution. The point stress criterion (Mc Clintock 1958; Whitney and Huismer 1974) states that fracture is initiated if the opening stress at a characteristic distance reaches a critical value. The average stress criterion (Novozhilov 1969; Seweryn 1994) assumes that failure occurs when the average opening stress over a characteristic length equals a critical value. In each case, the criterion does not refer to any energy balance and requires a tensile strength and a characteristic length which are supposed to be material properties, independent of geometry and stress distribution.

As proposed by Leguillon (2002), this approach can be improved by combining an energy and a stress condition to derive an initiation criterion. First, an energy balance between an elastic state prior to any crack growth and after the onset of a crack extension of area δS leads to

$$\delta W + \delta W_k + G^c \delta S = 0, \tag{1}$$

where $\delta W$is the change in potential energy, δW_k the change in kinetic energy and $G^c \delta S$ the fracture energy (G^c is the material toughness). Under the assumption of plane elasticity, the increment area is $\delta S = ae$ is where a is the crack length and e the specimen thickness. This energy balance leads to an incremental energy condition with

$$\delta W_k \geq 0 \Rightarrow -\frac{\delta W}{\delta S} = G^{inc}(a) = \overline{A}(a)\sigma^2 \geq G^c, \tag{2}$$

where σ is the remote applied stress and $G^{inc}(a)$ is the incremental energy release rate in which the infinitesimal energy rates of the classical Griffith approach are replaced by finite energy increments. If the scaling coefficient $\overline{A}(a)$ is an increasing function of the crack length (which can be numerically or asymptotically checked in many cases of stress concentration), the relation (2) provides a lower bound of the crack increment for a given value of the applied loading.

Second, a stress condition states that the opening normal stress σ_{op} along the anticipated path of crack nucleation is greater than the relevant strength σ^c:

$$\sigma_{op} = k_{op}(a)\sigma \geq \sigma^c. \tag{3}$$

If $k_{op}(a)$ is a decreasing function of the crack length (once again this can be numerically or asymptotically checked in many cases of stress concentration), relation (3) provides an upper bound of the crack increment for a given value of the applied loading. Increasing the loading reduces the lower bound but increases the upper bound. Finally, for a monotonic and increasing applied loading, the crack increment at nucleation a^* is obtained by combining the equalities in (2) and (3) which leads to

$$\frac{\overline{A}(a^*)}{\left(k_{op}(a^*)\right)^2} = \frac{G^c}{(\sigma^c)^2}, \tag{4}$$

The left hand side member of (4) is an increasing function of a^* vanishing for $a^* = 0$ so that this equation has always a solution and shows that the initiation length is not a material property but depends both on a characteristic fracture length $L^c = EG^c/(\sigma^c)^2$ (where E is the material modulus) and on the geometry of the structure. It will be seen in the following that in practice a^* is bounded by a structural value. Once the initiation length a^* is determined, the initiation stress σ^* equivalently derives either from the energy condition or from the stress condition with

$$\sigma^* = \frac{\sigma^c}{k_{op}(a^*)} = \sqrt{\frac{G^c}{\overline{A}\,(a^*)}}. \tag{5}$$

It is to be noted that this analysis allows to evaluate the initiation parameters (a^*, σ^*) which exactly fulfill $G^{inc}(a^*) = G^c$ so that the fracture event is not associated with any production of kinetic energy. One of the major drawback of the "finite fracture mechanics" approach is thus eliminated (Nairn 2001). Using the asymptotic expansion of the displacement field of the elastic solution, this approach was shown to provide a closed form expression which reveals accurate to predict the crack onset initiation at a sharp notch (Leguillon and Yosibash 2003). The approach was also recently used to study the fracture of a bond submitted to thermal loading (Muller et al. 2006). It is here applied to analyse the initiation of fracture mechanisms in the vicinity of a matrix crack within a composite cell.

3 The composite cell

The single fibre composite cylinder with axisymmetric boundary conditions which is often employed to understand the fibre/matrix interface behaviour is selected as a representative cell (Fig. 2a). This model considers a single fibre of radius R_f surrounded by a cylinder of matrix having an inner radius R_f and outer radius R_m such that the area fraction of the fibre is $V_f = \left(R_f/R_m\right)^2$. A set of cylindrical polar coordinates (r, θ, z) is selected so that the z axis corresponds to the axis of the fibre with the origin taken to be at the centre of the cell. The half length L of the cell is $L = 10R_f$. A matrix crack normal to the fibre direction is located in the plane $z = 0$ and the ligament width between the crack tip and the fibre/matrix interface is denoted by ℓ. Multiple matrix cracking is not taken into account here as we

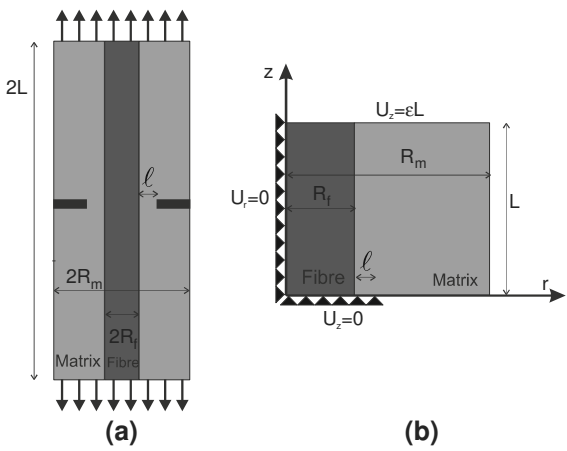

Fig. 2 The simple fibre composite cylinder submitted to a uniform axial strain: (**a**) location of the annular matrix crack and (**b**) boundary conditions of the numerical model

only consider the early stage of damage development. This composite cylinder is submitted to a uniform remote axial strain ε. The lateral surface $r = R_m$ is stress free and a perfect interfacial bonding is assumed. The fibre and matrix materials are taken to be elastic and isotropic with Young's moduli (E_f, E_m) and Poisson's ratios (ν_f, ν_m). A numerical model (with the boundary conditions indicated by Fig. 2b) was used in order to obtain displacement based finite element solutions as detailed in the Appendix. The values $R_f = 7.5\,\mu$m, $E_f = 100\,$GPa, $\nu_f = \nu_m = 0.2$, and $V_f = 0.4$ were selected as typical values for the calculations. The dimensionless ligament width ℓ/R_f was taken within the range (0.6–6%). Closure of the interfacial crack was checked but was not observed for the simulated debond lengths $2d$ with $d/\ell \leq 10$.

For a given ligament width ℓ, the stress concentration induced by the matrix crack is evidenced by plotting (Fig. 3) the radial stress $\sigma_{rr}(\ell, z)$ along the fibre/matrix interface and the axial stress $\sigma_{zz}(\ell, r)$ in the fibre which are given by

$$\begin{aligned} \sigma_{rr}(\ell, z) &= k_{rr}(\ell, z) E_i \varepsilon, \\ \sigma_{zz}(\ell, r) &= k_{zz}(\ell, r) E_f \varepsilon, \end{aligned} \tag{6}$$

where (k_{rr}, k_{zz}) are stress concentration factors and E_i is the effective modulus defined by $2/E_i = (1 - \nu_f^2/E_f) + (1 - \nu_m^2/E_m)$ which enters the energy release rate expression for an interfacial crack between two semi-infinite and different elastic materials (Hutchinson et al. 1987).

The energy release rates (G_m, G_d, G_p) (i.e. the derivatives of the potential energy with respect to the crack area) for the propagation of respectively a matrix crack, an interfacial

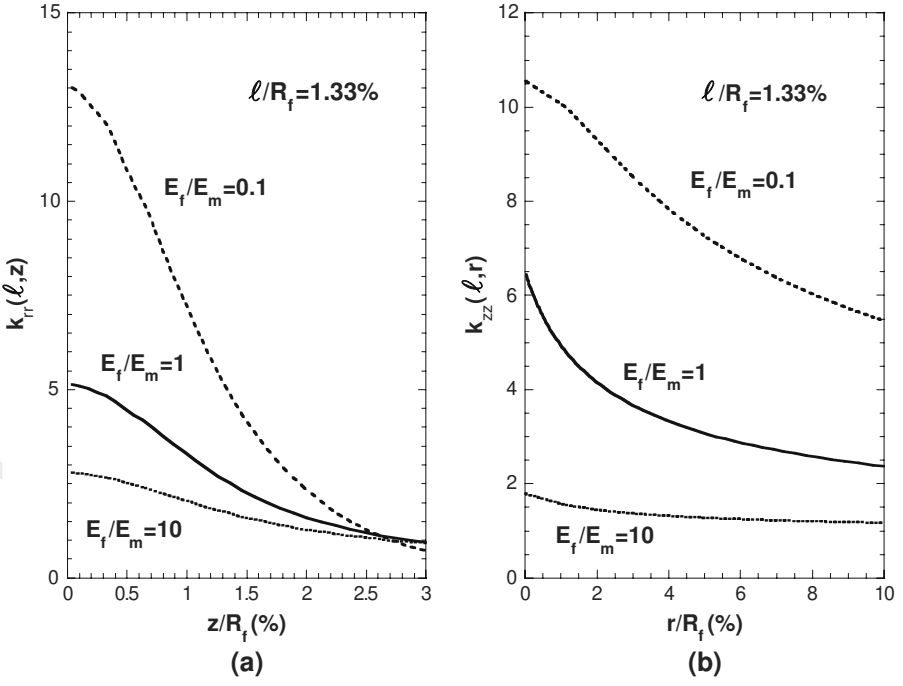

Fig. 3 Stress concentration induced by the matrix crack: (**a**) radial stress concentration factor along the interface and (**b**) axial stress concentration factor in the fibre

crack of length $2d$ and a fibre penetrating crack of length p are estimated with the help of a crack closure method. The following relationships

$$\begin{aligned} G_m(\ell) &= A_m(\ell) R_f E_f \varepsilon^2, \\ G_d(\ell, d) &= A_d(\ell, d) R_f E_i \varepsilon^2, \\ G_p(\ell, p) &= A_p(\ell, p) R_f E_f \varepsilon^2, \end{aligned} \tag{7}$$

allow defining the coefficients $\left(A_m(\ell), A_d(\ell, d), A_p(\ell, p)\right)$ as dimensionless energy release rates. Then, the incremental energy release rates $\left(G_d^{inc}, G_p^{inc}\right)$ for decohesion and penetration mechanisms are deduced from

$$\begin{aligned} G_d^{inc}(\ell, d) &= \frac{1}{\delta S_d} \int_0^d G_d(\ell, d) dS_d = \overline{A_d}\,(\ell, d)\, R_f E_i \varepsilon^2, \\ G_p^{inc}(\ell, p) &= \frac{1}{\delta S_p} \int_0^p G_p(\ell, p)\, dS_p = \overline{A_p}(\ell, d) R_f E_f \varepsilon^2, \end{aligned} \tag{8}$$

where $\delta S_d = \int_0^d dS_d$, $\delta S_p = \int_0^p dS_p$ are the corresponding increment areas.

Figure 4 illustrates the evolution of the dimensionless energy release rates $(A_m(\ell), \overline{A}_d(\ell, d), \overline{A}_p(\ell, p))$ versus the relevant crack lengths and shows that higher values are always obtained if $E_f/E_m < 1$. In the following, the coefficients $(k_{rr}(\ell, z), k_{zz}(\ell, z))$ and $\left(A_m(\ell), \overline{A}_d(\ell, d), \overline{A}_p(\ell, p)\right)$ estimated with the help of the numerical model are used in order to determine the applied strain ε_m^* at initiation of the matrix crack propagation and the applied strains $\left(\varepsilon_p^*, \varepsilon_d^*\right)$ at initiation of penetration and debonding.

4 Results and discussion

4.1 Propagation of the matrix crack

As already discussed by previous authors (Leguillon and Sanchez-Palencia 1992), Fig. 4a shows that the discontinuity in the elastic properties strongly modifies the behaviour of the energy release rate of the matrix crack in the vicinity of the interface. In the case of a weak singularity ($E_f/E_m > 1$), the non-dimensional energy release rate $A_m(\ell)$ decreases to 0 if the ligament width reduces. Reversely, a strong singularity ($E_f/E_m < 1$) implies that $A_m(\ell)$ tends to infinity. The use of the classical Griffith condition $G_m(\ell) = G_m^c$ (where G_m^c is the matrix toughness) allows evaluating the applied strain $\varepsilon_m^*(\ell)$ at initiation of the matrix crack with

$$\varepsilon_m^*(\ell) = \left[\frac{G_m^c}{A_m(\ell) E_f R_f}\right]^{1/2}. \tag{9}$$

As expected, relation (9) shows that matrix crack propagation is inhibited (respectively enhanced) by a stiffer (respectively softer) fibre.

4.2 Initiation of fibre cracking

Considering the fibre cracking mechanism, the initiation criterion (2)(3) provides the following conditions

$$\begin{aligned} G_p^{inc}(\ell, p) &= \overline{A}_p(\ell, p) E_f R_f \varepsilon^2 \geq G_f^c, \\ \sigma_{zz}(\ell, p) &= k_{zz}(\ell, p) E_f \varepsilon \geq \sigma_f^c, \end{aligned} \tag{10}$$

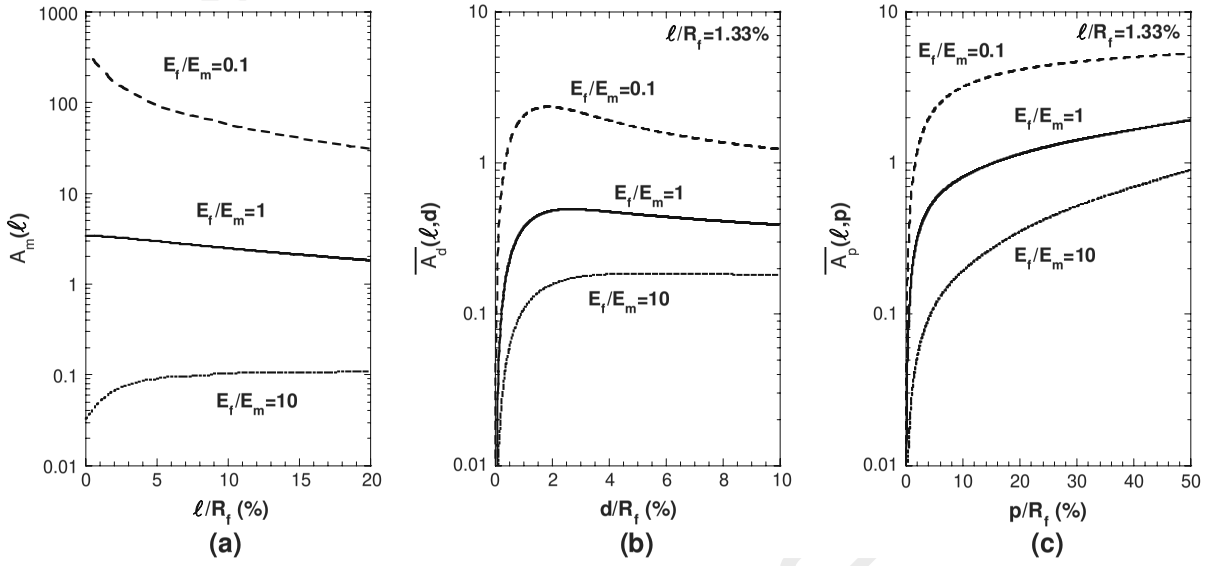

Fig. 4 Non-dimensional energy release rates: (**a**) normalised value of the energy release rate of the matrix crack versus the ligament width, (**b**) normalised value of the incremental energy release rate of the interfacial crack versus the debonding length, and (**c**) normalised value of the incremental energy release rate of the penetrating crack versus the penetration length

where G_f^c and σ_f^c denote respectively the fibre toughness and the fibre tensile strength. As is made clear by Fig. 4c, $\overline{A}_p(\ell, p)$ is an increasing function of p for a given value of the ligament. Introducing the characteristic fracture length of the fibre $L_f^c = (E_f G_f^c)/(\sigma_f^c)^2$ and using (4) allows to determine the penetrating length at initiation p^* by solving

$$\frac{\overline{A}_p(\ell, p*)}{k_{zz}^2(\ell, p*)} = \frac{L_f^c}{R_f}. \tag{11}$$

For small values of L_f^c such that $L_f^c/R_f \ll 1$, results show that the initiation length remains small with $p^*/R_f \ll 1$. If the fibre toughness tends toward low values with the limiting case $G_f^c \to 0$, the energetic condition is easily satisfied and the initiation criterion tends towards the stress condition with

$$\lim_{G_f^c \to 0} \varepsilon_p^*(\ell) = \varepsilon_p^S(\ell) = \frac{\sigma_f^c}{E_f k_{zz}(\ell, 0)}. \tag{12}$$

The left hand size of (11) is an increasing function of p^* which implies that larger is the characteristic length L_f^c and larger is the initiation length p^*. The whole fibre will be fractured at initiation with $p^* = R_f$ if L_f^c is high enough with

$$L_f^c \geq L_p^{\max}(\ell) = \frac{\overline{A}_p(\ell, R_f)}{k_{zz}^2(\ell, R_f)} R_f. \tag{13}$$

Assuming that the energy condition is satisfied with $\overline{A}_p(\ell, R_f) E_f R_f \varepsilon^2 = G_f^c$ and rewriting (13) as

$$\frac{E_f G_f^c}{R_f} \frac{k_{zz}^2(\ell, R_f)}{\overline{A}_p(\ell, R_f)} \geq \left(\sigma_f^c\right)^2$$

implies that the stress condition is always fulfilled because

$$\left(\sigma_{zz}(\ell, R_f)\right)^2 = \left(k_{zz}(\ell, R_f) E_f \varepsilon\right)^2 = \frac{E_f G_f^c}{R_f} \frac{\left(k_{zz}(\ell, R_f)\right)^2}{\overline{A}_p(\ell, R_f)} \geq \left(\sigma_f^c\right)^2. \tag{14}$$

If the characteristic fracture length of the fibre is large enough as required by (13) with $L_f^c \geq L_p^{\max}$, then the energy condition is the governing one and the applied strain at initiation of fibre cracking ε_p^* is

$$\varepsilon_p^*(\ell) = \varepsilon_p^w(\ell) = \left[\frac{G_f^c}{\overline{A}_p(\ell, R_f) E_f R_f}\right]^{1/2}. \tag{15}$$

The structural length $L_p^{\max}$ must be compared with the material length L_f^c in order to obtain the main features of the penetration mechanism. Figure 5a which plots $L_p^{\max}$ versus ℓ indicates that condition (13) is more easily satisfied for a large ligament width and a soft fibre. As summarized by Fig. 6 which depicts the applied strain at initiation $\varepsilon_p^*/\varepsilon_p^w$ and the initiation length p^*/R_f versus the length ratio $L_f^c/L_p^{\max}$, two cases must be differentiated:

(i) *a strong but brittle fibre* (i.e. a high σ_f^c and a low G_f^c) with $L_f^c < L_p^{\max}$: the initiation length is reduced ($p^* < R_f$) but the applied strain at initiation is increased ($\varepsilon_p^* > \varepsilon_p^w$).

(ii) *a tough but weak fibre* (i.e. a high G_f^c and a low σ_f^c) with $L_f^c \geq L_p^{\max}$: the energy condition (15) is dominating so that the initiation length reaches its maximum value $\left(p^* = R_f\right)$.

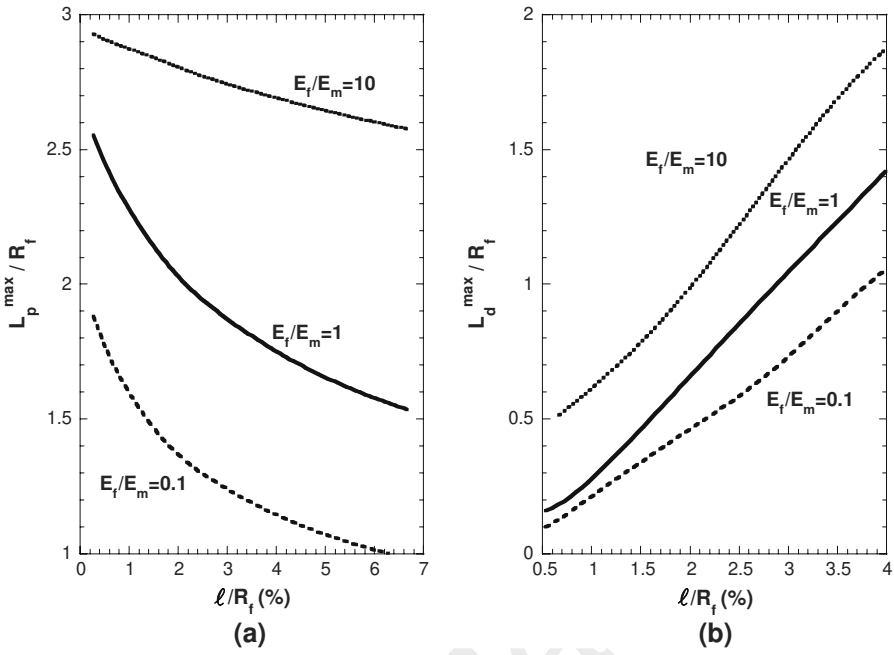

Fig. 5 The structural parameters $L_p^{\max}$ and $L_d^{\max}$ versus the ligament width

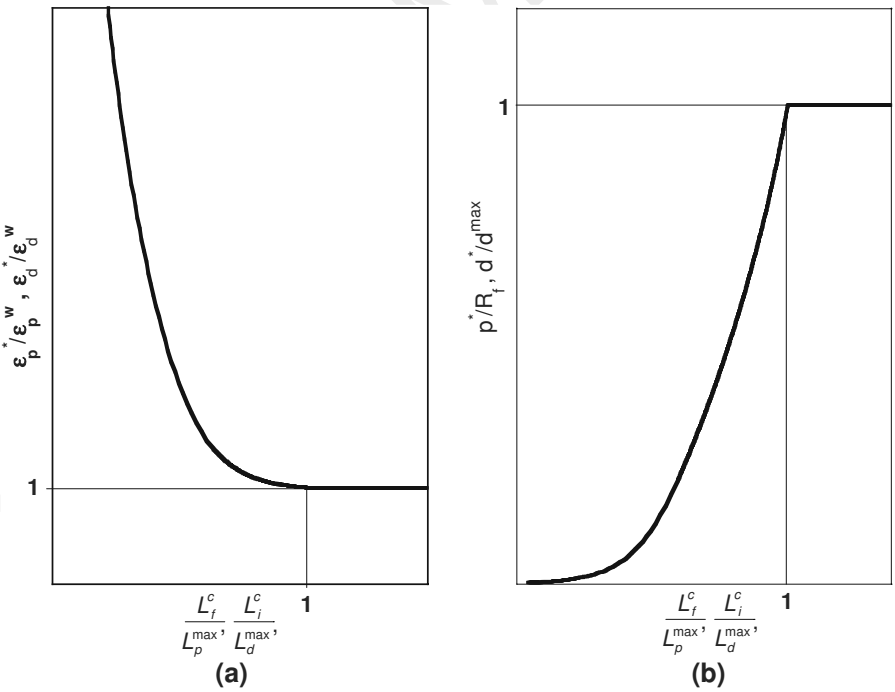

Fig. 6 Initiation of the fracture mechanisms: (**a**) schematic of the applied strain at initiation versus the $L^c/L^{\max}$ ratio and (**b**) schematic of the initiation length versus the $L^c/L^{\max}$ ratio

4.3 Initiation of interfacial debonding

In the case of interfacial debonding, results in Fig. 4b indicate that the incremental energy release rate always exhibits a maximum value for $z = d^{\max}(\ell)$. Thus, for a monotonically increasing applied strain, the energy condition (2) is first satisfied if

$$G_d^{inc}(\ell, d) = \overline{A}_d(\ell, d^{\max}) E_i R_f \varepsilon^2 = G_i^c, \tag{16}$$

where G_i^c is the interfacial toughness. The initiation of a debonding crack of half length $d^{\max}$ also requires the stress condition (3) to be satisfied with

$$\sigma_{rr}(\ell, d^{\max}) = k_{rr}(\ell, d^{\max}) E_i \varepsilon \geq \sigma_i^c, \tag{17}$$

where σ_i^c is the tensile interfacial strength. The inequality (17) with (16) implies

$$L_i^c \geq L_d^{\max}(\ell) = \frac{\overline{A}_d(\ell, d^{\max})}{k_{rr}^2(\ell, d^{\max})} R_f, \tag{18}$$

where the interfacial characteristic fracture length $L_i^c = E_i G_i^c / (\sigma_i^c)^2$ and the structural length $L_d^{\max}$ are introduced. It is interesting to note that (Pronin and Gupta 1998) suggest correlating the length L_i^c with the interatomic separation distance across the interface. Comparing L_i^c and $L_d^{\max}$ allows to distinguish between two different situations:

(i) *a tough but weak interface* (i.e. a high G_i^c and a low σ_i^c) results in a high value of the interfacial characteristic length with $L_i^c \geq L_d^{\max}$. In this case, the stress condition (17) is always satisfied and the energy condition (16) is the governing one. The debonded length at initiation is a structural parameter $d^* = d^{\max}$ which does not depend on the interfacial fracture properties. The applied strain at initiation of debonding does not depend on the interfacial strength and is given by

$$\varepsilon_d^*(\ell) = \varepsilon_d^w(\ell) = \left[\frac{G_i^c}{\overline{A}_d(\ell, d^{\max}) E_i R_f} \right]^{1/2}. \tag{19}$$

(ii) *a strong but brittle interface* (i.e. a high σ_i^c and a low G_i^c) induces a low value of the interfacial characteristic length with $L_i^c < L_d^{\max}$. In this case, the debonded length at initiation d^* is obtained by solving

$$\frac{\overline{A}_d(\ell, d^*)}{k_{rr}^2(\ell, d^*)} = \frac{L_i^c}{R_f}, \tag{20}$$

which shows that d^* is lower than $d^{\max}$ and now depends on the structural geometry and the fracture properties. In the limiting case $G_i^c \to 0$, the energetic condition is always satisfied and the initiation criterion tends towards the stress condition with

$$\lim_{G_i^c \to 0} \varepsilon_d^*(\ell) = \varepsilon_d^S(\ell) = \frac{\sigma_i^c}{E_i k_{rr}(\ell, 0)}. \tag{21}$$

The structural length $L_d^{\max}(\ell)$ which delineates the frontier between "high" and "low" values of the interfacial characteristic length is plotted in Fig. 5b. It is interesting to note that $L_d^{\max}(\ell)$ decreases with lower values of the ligament width and a soft fibre so that (18) is more easily satisfied in this case. Figure 6 schematically depicts the applied strain at initiation $\varepsilon_d^*/\varepsilon_d^w$ and the initiation length $d^*/d^{\max}$ versus the normalized interfacial strength $L_i^c/L_d^{\max}$ in order to exhibit the main features of the decohesion mechanism (which are similar to

those obtained for the penetration one). For large values of the characteristic length such that $L_i^c \geq L_d^{\max}$, the energy condition (19) is dominating and the initiation length reaches its maximum value $d^{\max}$. Reducing the characteristic length such that $L_i^c < L_d^{\max}$ leads to an increase of the applied strain at initiation and reduces the initiation length.

Following the analysis of each fracture mechanism, the competition between matrix cracking, interfacial debonding and fibre penetration can now be straightforwardly examined. It is assumed here that the matrix crack is stationary and that the representative cell is submitted to a monotonic tensile loading so that a given mechanism will be promoted if the corresponding applied strain at initiation is the lowest.

4.4 Competition between matrix cracking and fibre penetration or interfacial debonding

- Compared to matrix crack propagation, fibre penetration is promoted if

$$\varepsilon_p^*(\ell) < \varepsilon_m^*(\ell), \tag{22}$$

where ε_m^* is provided by (9). Figure 7a, b show the relevant mechanism map in the plane $\left(G_m^c, G_f^c\right)$ with $E_f/E_m = 1$ for a fixed value of the ligament width and various values of the fibre strength. The penetration domain is located below the curves. As expected, the penetration mechanism is more difficult for strong fibres. Figure 7a, b reveal the presence of (i) a matrix toughness threshold which increases with the fibre strength and which must be exceeded to allow the penetration mechanism, (ii) a linear part of the frontier for which the penetration criterion is then reduced to an energy criterion (i.e. $G_f^c/G_m^c <$ fixed value). Those specific features are now explained by comparing the lengths L_f^c and $L_p^{\max}$ as suggested by the results of Sect. 4.2.

For the highest values of the fibre fracture length such that $L_f^c \geq L_p^{\max}$, the penetration into the fibre is only driven by the energy condition (15) so that the penetration criterion (22) turns out to

$$G_f^c < W_{pm}(\ell) G_m^c \quad \text{with} \quad W_{pm}(\ell) = \frac{\overline{A_p}(\ell, R_f)}{A_m(\ell)}. \tag{23}$$

Relation (23) corresponds to the linear part of Fig. 7b. In this case, the whole fibre is fractured at initiation with $p^* = R_f$.

Reducing the fibre fracture length such that $L_f^c < L_p^{\max}$ decreases the initiation length p^* which becomes smaller than R_f. The stress condition (12) holds for the limiting case $G_f^c \to 0$ so that the penetration criterion (22) becomes

$$\left(\frac{\sigma_f^c}{E_f k_{zz}(\ell, 0)}\right)^2 < \frac{G_m^c}{E_f R_f A_m(\ell)} \text{ or } 1 < \frac{G_m^c}{G_p^{th}(\ell)} \text{ with } G_p^{th}(\ell) = \frac{A_m(\ell)}{k_{zz}^2(\ell, 0)} \frac{R_f\left(\sigma_f^c\right)^2}{E_f}. \tag{24}$$

Relation (24) demonstrates that the matrix crack propagation is always favoured if the matrix toughness G_m^c is smaller than G_p^{th} which is the matrix toughness threshold observed in Fig. 7a. For a given value of the matrix toughness, fibre penetration is inhibited if the fibre strength is larger than a strength threshold σ_p^{th} defined by

$$\sigma_p^{th}(\ell) = \left[\frac{(k_{zz}(\ell, 0))^2}{A_m(\ell)} \frac{E_f}{R_f} G_m^c\right]^{1/2}. \tag{25}$$

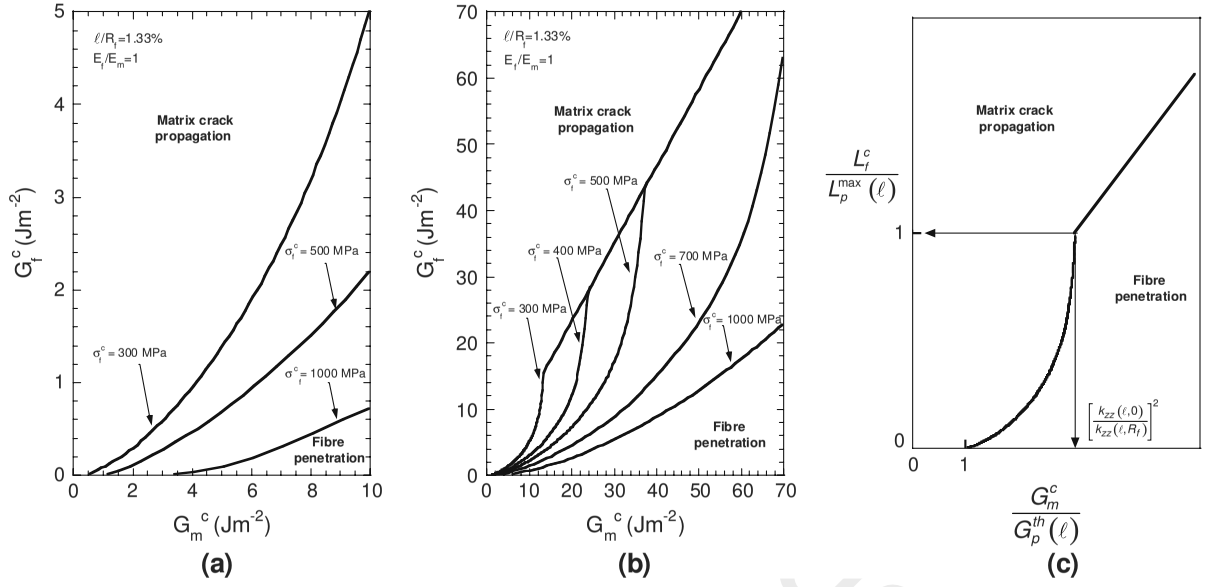

Fig. 7 Competition between matrix cracking and fibre penetration: (**a**) and (**b**) propagation/penetration domain in the plane (G_m^c, G_f^c) for $E_f/E_m = 1$ and $\ell/R_f = 1.33\%$, and (**c**) schematic of the propagation/penetration domain in the normalised plane $(G_m^c/G_p^{th}, L_f^c/L_p^{\max})$

To summarize these results, Fig. 7c schematizes the mechanism map in the normalized plane $(G_m^c/G_p^{th}, L_f^c/L_p^{\max})$ for a given value of the ligament. The penetration domain is limited by a concave part if $L_f^c < L_p^{\max}$ whereas the linear curve (23) is obtained if $L_f^c \geq L_p^{\max}$. It is to be noted that the slope of the linear part is now

$$\left[\frac{k_{zz}(\ell, R_f)}{k_{zz}(\ell, 0)}\right]^2$$

as a consequence of the normalisation choice.

- The competition between matrix cracking and interfacial debonding is now analysed. Interfacial debonding will occur preferentially to matrix cracking if

$$\varepsilon_d^*(\ell) < \varepsilon_m^*(\ell). \tag{26}$$

Figure 8a plots the related mechanism map in the plane (G_m^c, G_i^c) with $E_f/E_m = 1$ for a fixed value of the ligament width and various values of the interfacial strength. The decohesion domain is located below the curves. As could be intuitively expected, the deflection is easier for weak interfaces. Figure 8a indicates that each boundary includes in the bottom a matrix toughness threshold which must be exceeded to allow interfacial debonding and a convex part followed by a linear curve. In this last case, the deflection criterion takes the form of an energy condition (i.e. $G_i^c/G_m^c <$ fixed value). The results of Sect. 4.3 are now used to recover those features by comparing the lengths L_i^c and $L_d^{\max}$.

For higher values of the interfacial fracture length such that $L_i^c \geq L_d^{\max}$, the decohesion is driven by the energy condition (19) so that the decohesion criterion is $\varepsilon_d^w(\ell) < \varepsilon_m^*(\ell)$ which leads to

$$G_i^c \leq W_{dm}(\ell) G_m^c \quad \text{with} \quad W_{dm}(\ell) = \frac{E_i}{E_f} \frac{\overline{A_d}\,(\ell, d^{\max})}{A_m(\ell)}. \tag{27}$$

Relation (27) corresponds to the linear part in Fig. 8a. In this case the initiation length reaches its maximum value with $d^* = d^{\max}$. Lowest values of the interfacial fracture length with $L_i^c < L_d^{\max}$leads to the convex part in Fig. 8a with $d^* < d^{\max}$. The stress condition (21) must be used for the limiting case $G_i^c \to 0$ so that (26) becomes

$$\left(\frac{\sigma_i^c}{E_i k_{rr}(\ell, 0)}\right)^2 < \frac{G_m^c}{E_f R_f A_m(\ell)} \quad \text{or} \quad 1 < \frac{G_m^c}{G_d^{th}(\ell)}$$
$$\text{with} \quad G_d^{th}(\ell) = \frac{E_f}{E_i} \frac{A_m(\ell)}{k_{rr}^2(\ell, 0)} \frac{R_f (\sigma_i^c)^2}{E_i}. \tag{28}$$

Relation (28) defines the matrix toughness threshold G_d^{th} which is exhibited in Fig. 8a. For a given value of the matrix toughness, the interfacial decohesion is only possible if the interface strength is smaller than a strength limit σ_d^{th} defined by

$$\sigma_d^{th}(\ell) = \left[\frac{(k_{rr}(\ell, 0))^2}{A_m(\ell)} \frac{(E_i)^2}{E_f R_f} G_m^c\right]^{1/2}. \tag{29}$$

To summarize these results, Fig. 8b schematizes the mechanism map in the normalized plane $(G_m^c/G_d^{th}, L_i^c/L_d^{\max})$ for a given value of the ligament width. The normalizing factor G_d^{th} is used and the debonding domain is located below the curve. The boundary is convex if $L_i^c < L_d^{\max}$ but the linear curve (23) is obtained as soon as $L_i^c \geq L_d^{\max}$. It is to be noted that

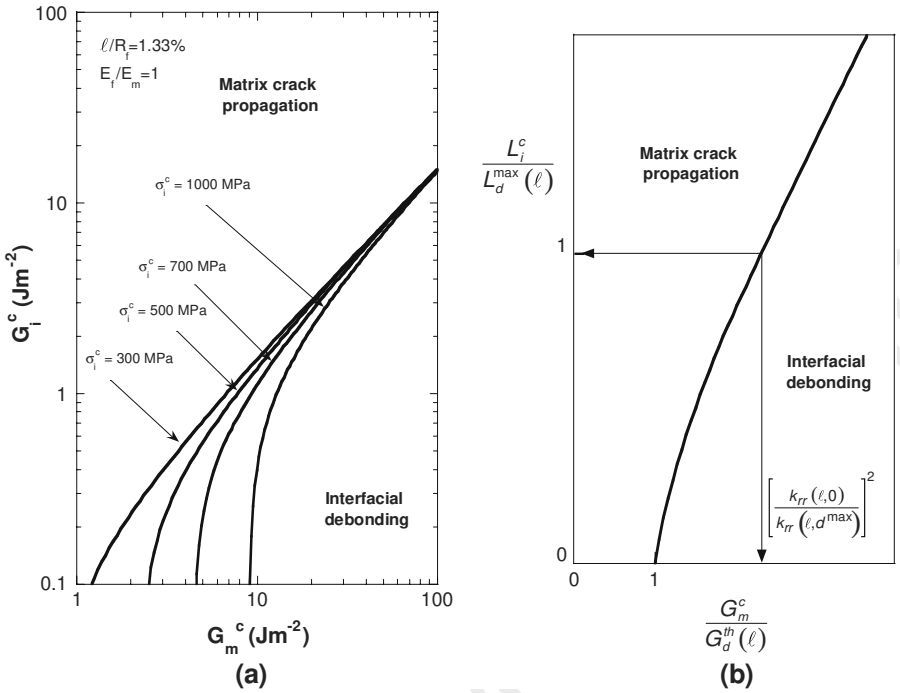

Fig. 8 Competition between matrix cracking and interfacial debonding: (**a**) propagation/debonding domain in the plane (G_m^c, G_i^c) for $E_f/E_m = 1$ and $\ell/R_f = 1.33\%$ and (**b**) schematic of the propagation/penetration domain in the normalised plane $(G_m^c/G_d^{th}, L_i^c/L_d^{\max})$

the slope of the linear part is now $\left[k_{rr}(\ell, d^{\max})/k_{rr}(\ell, 0)\right]^2$ as a consequence of the normalisation choice. For a weak singularity $\left(E_f/E_m > 1\right)$, results show that the structural parameters $\left(W_{dm}, W_{pm}\right)$ exhibit higher values which favours interface debonding or fibre penetration because the matrix crack propagation is inhibited in this case as already mentioned in Sect. 4.1.

4.5 Competition between interfacial debonding and fibre cracking

Ignoring now the possibility of matrix crack propagation, the competition between interfacial debonding and fibre penetration is analysed. The decohesion will be predicted if the applied strain at initiation of debonding is lower than the applied strain at initiation of penetration

$$\varepsilon_d^*(\ell) < \varepsilon_p^*(\ell). \tag{30}$$

The decohesion/penetration domain now depends on the full set of fracture parameters $(G_f^c, \sigma_f^c, G_i^c, \sigma_i^c)$. Selecting the (G_f^c, G_i^c) plane, Fig. 9 shows a mechanism map for $E_f/E_m = 1$ and a fixed value of the ligament width. The boundary of the penetration/decohesion domain is computed for a fixed value of the interfacial strength ($\sigma_i^c = 500\,\text{MPa}$) and various values of the fibre strength. As one could expect, decohesion is promoted by a weak value of the strength ratio σ_i^c/σ_f^c. Figure 9 reveals the presence of (i) a fibre toughness threshold for large values of σ_i^c/σ_f^c, (ii) an interfacial toughness threshold for low values of σ_i^c/σ_f^c, (iii) a linear part of the boundary for which the decohesion criterion reduces to an

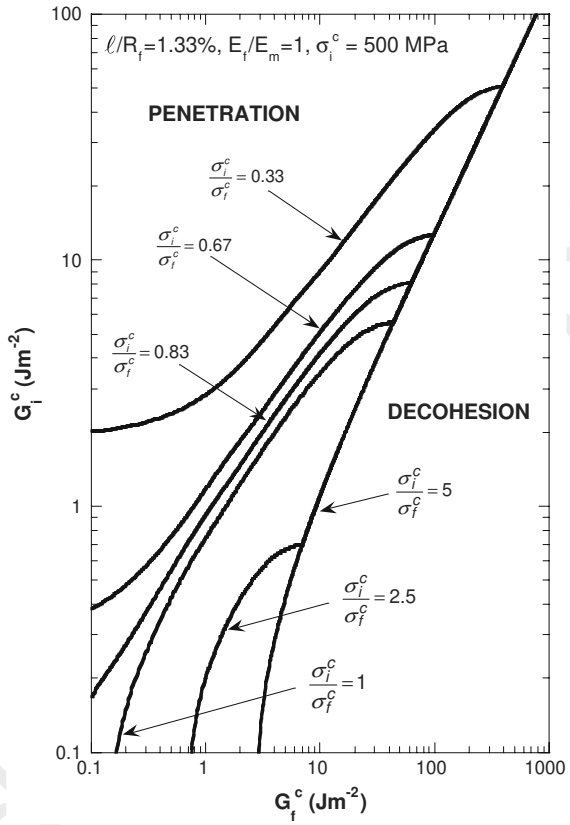

Fig. 9 Competition between fibre penetration and interfacial debonding: the penetration/debonding domain is plotted in the plane $(G_f^c, G_i^c)$for $E_f/E_m = 1$, $\ell/R_f = 1.33\%$ and $\sigma_i^c = 500\,\text{MPa}$

energy criterion (i.e. $G_i^c/G_f^c <$ fixed value). Those characteristics features will be evidenced in the sequel by comparing the characteristic fracture lengths $\left(L_f^c, L_i^c\right)$ with the structural lengths $\left(L_d^{\max}, L_p^{\max}\right)$.

First, it is assumed that the penetration mechanism is only controlled by the energy condition (15). This implies that large values of L_f^c are selected with $L_f^c \geq L_p^{\max}$and thus fibre toughness values such that

$$G_f^c \geq L_p^{\max}(\ell)\frac{\left(\sigma_f^c\right)^2}{E_f}. \tag{31}$$

In the limiting case $G_i^c \to 0$, the condition for decohesion tends towards the stress condition (21) so that the decohesion criterion (30) reads

$$G_f^c \geq \frac{\overline{A}_p(\ell, R_f)}{k_{rr}^2(\ell, 0)}\frac{R_f E_f}{E_i^2}(\sigma_i^c)^2 = \gamma_1(\ell)\frac{R_f E_f}{E_i^2}(\sigma_i^c)^2 = G_f^{th}(\ell), \tag{32}$$

which introduces the fibre toughness threshold G_f^{th} (depending on σ_i^c through the structural parameter $\gamma_1(\ell)$) observed in Fig. 9. Relations (31) and (32) provide two different lower limits for G_f^c but (32) is sufficient if it is assumed that

$$\frac{\sigma_i^c}{\sigma_f^c} \geq \delta_1(\ell) = \frac{E_i}{E_f}\frac{k_{rr}(\ell,0)}{k_{zz}(\ell,R_f)}. \tag{33}$$

For a given value of the fibre strength, a "strong" interface can thus be defined by (33). Keeping σ_i^c in order to satisfy (33) but increasing G_i^c such that $L_i^c \geq L_d^{\max}$ with $G_i^c \geq L_d^{\max}\frac{(\sigma_i^c)^2}{E_i}$ allows using the energy condition (19) to describe the initiation of decohesion so that the criterion (30) becomes

$$G_i^c < \frac{E_i}{E_f}\frac{\overline{A_d}(\ell, d^{\max})}{\overline{A_p}(\ell, R_f)}G_f^c = W_{dp}(\ell)G_f^c \quad \text{with} \quad W_{dp}(\ell) = \frac{W_{dm}(\ell)}{W_{pm}(\ell)}. \tag{34}$$

Figure 10a plots the relevant decohesion/penetration domain obtained for the values of the ratio σ_i^c/σ_f^c defined by (33). The data are plotted in the plane $(G_f^c/G_f^{th}, L_i^c/L_d^{\max})$. As expected from (34), a linear curve is obtained as soon as $L_i^c/L_d^{\max} \geq 1$ which means that both mechanisms are only controlled by the energy condition. A convex curve is observed if $L_i^c/L_d^{\max} < 1$ and penetration is always predicted if the fibre toughness is lower than the threshold G_f^{th} defined by (32). In this case, the penetration mechanism is always activated whatever the value of G_i^c provided that $G_f^c < G_f^{th}$. This result demonstrates that a low toughness interface is not systematically a sufficient condition to promote the initiation of deflection.

Second, it is now assumed that the debonding mechanism is only controlled by the energy condition (19). Large values of L_i^c with $L_i^c \geq L_d^{\max}$ and thus interfacial toughness values such that

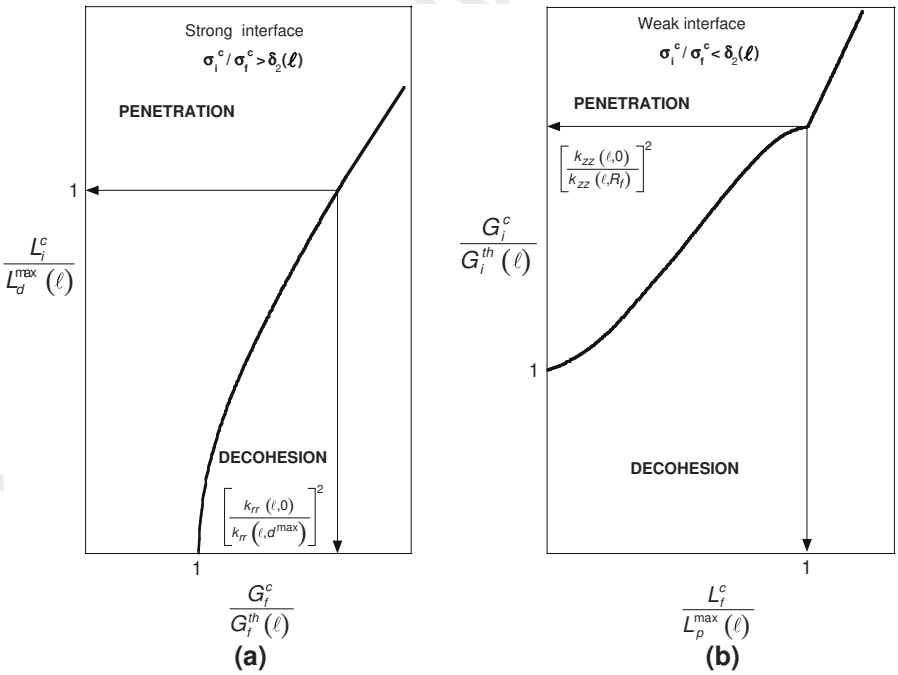

Fig. 10 Competition between fibre penetration and interfacial debonding. Schematic of the penetration/debonding domain for: (**a**) $\sigma_i^c/\sigma_f^c > \delta_1(\ell)$ in the normalised plane $(G_f^c/G_f^{th}, L_i^c/L_d^{\max})$ and (**b**) $\sigma_i^c/\sigma_f^c < \delta_2(\ell)$ in the normalised plane $(L_f^c/L_p^{\max}, G_i^c/G_i^{th})$

$$G_i^c \geq L_d^{\max} \frac{(\sigma_i^c)^2}{E_i} \tag{35}$$

are selected. For small values of the fibre toughness such that $G_f^c \to 0$, the initiation of penetration is mainly dependant on the stress condition (12) so that the penetration criterion $\varepsilon_d^* > \varepsilon_p^*$ reads

$$G_i^c \geq \frac{\overline{A}_d(\ell, d^{\max})}{k_{zz}^2(\ell, 0)} \frac{R_f E_i}{E_f^2} \left(\sigma_f^c\right)^2 = \gamma_2(\ell) \frac{R_f E_i}{E_f^2} \left(\sigma_f^c\right)^2 = G_i^{th}(\ell). \tag{36}$$

Relation (36) defines the interfacial toughness threshold G_i^{th} (depending on σ_f^c through the structural parameter $\gamma_2(\ell)$) observed in Fig. 9. Two different lower limits are provided by (35) and (36) for G_i^c but (36) is sufficient if it is assumed that

$$\frac{\sigma_i^c}{\sigma_f^c} \leq \delta_2(\ell) = \frac{E_i}{E_f} \frac{k_{rr}(\ell, d^{\max})}{k_{zz}(\ell, 0)}. \tag{37}$$

For a fixed value of the fibre strength, relation (37) defines a "weak" interface. Keeping σ_f^c in order to satisfy (36) but increasing G_f^c such that $L_f^c \geq L_p^{\max}$ requires that $G_f^c \geq L_p^{\max} \frac{\left(\sigma_f^c\right)^2}{E_f}$. In this case, the energy condition (15) can be used to describe the initiation of penetration so that the penetration criterion $\varepsilon_p^* < \varepsilon_d^*$ becomes

$$G_f^c < \frac{E_f}{E_i} \frac{\overline{A_p}(\ell, R_f)}{\overline{A_d}(\ell, d^{\max})} G_i^c = \frac{1}{W_{dp}(\ell)} G_i^c. \tag{38}$$

Figure 10b depicts the corresponding failure map now obtained for the values of the ratio σ_i^c/σ_f^c which satisfy (37). The data are plotted in the plane $\left(L_f^c/L_p^{\max}, G_i^c/G_i^{th}\right)$. As expected from (38), a linear curve is obtained as soon as $L_f^c/L_p^{\max} \geq 1$ which means that both mechanisms are controlled by the energy condition. A different behaviour is observed if $L_f^c/L_p^{\max} < 1$ and decohesion is always possible if the interfacial toughness is smaller than the threshold G_i^{th} defined by (36) whatever the value of G_f^c. This result indicates that the initiation of deflection can be achieved even if the fibre toughness is low.

The decohesion/penetration maps represented by Fig. 10 were obtained under the general assumption that at least one of the mechanism is controlled by the energy condition. In this case, only three fracture parameters $(G_f^c, G_i^c, \sigma_i^c)$ or $(G_f^c, G_i^c, \sigma_f^c)$ are needed. For intermediate values of the ratio σ_i^c/σ_f^c such that $\delta_2 < \sigma_i^c/\sigma_f^c < \delta_1$, the full set of the fracture parameters $(G_f^c, \sigma_f^c, G_i^c, \sigma_i^c)$ is involved as already shown by Fig. 9 which exhibits a gradual transition between the two previous regimes.

Influence of the modulus ratio and the ligament width on the competition between interfacial decohesion and penetration is analysed in Fig. 11. Figure 11a which plots δ_1 versus the ligament width indicates that obtaining a "strong" interface (as defined by (33)) is easier with a stiff fibre because δ_1 decreases with the modulus ratio. Nevertheless, Fig. 11b shows that in this case a higher value of the fibre toughness threshold G_f^{th} is necessary to prevent penetration. Conversely, defining a "weak" interface (following relation (37)) is facilitated by a soft fibre as δ_2 is higher in this case (Fig. 11c) but decohesion then requires a low value of the interfacial toughness threshold G_i^{th} (Fig. 11d). For ceramic matrix composites (Domergue et al. 1995), the elastic mismatch is moderate and the typical values $\left(\sigma_f^c \approx 1\text{–}4\,\text{GPa}\right)$ and $\left(\sigma_i^c \approx 50\text{–}300\,\text{MPa}\right)$ allow to satisfy the "weak" interface condition (37). Consequently, the

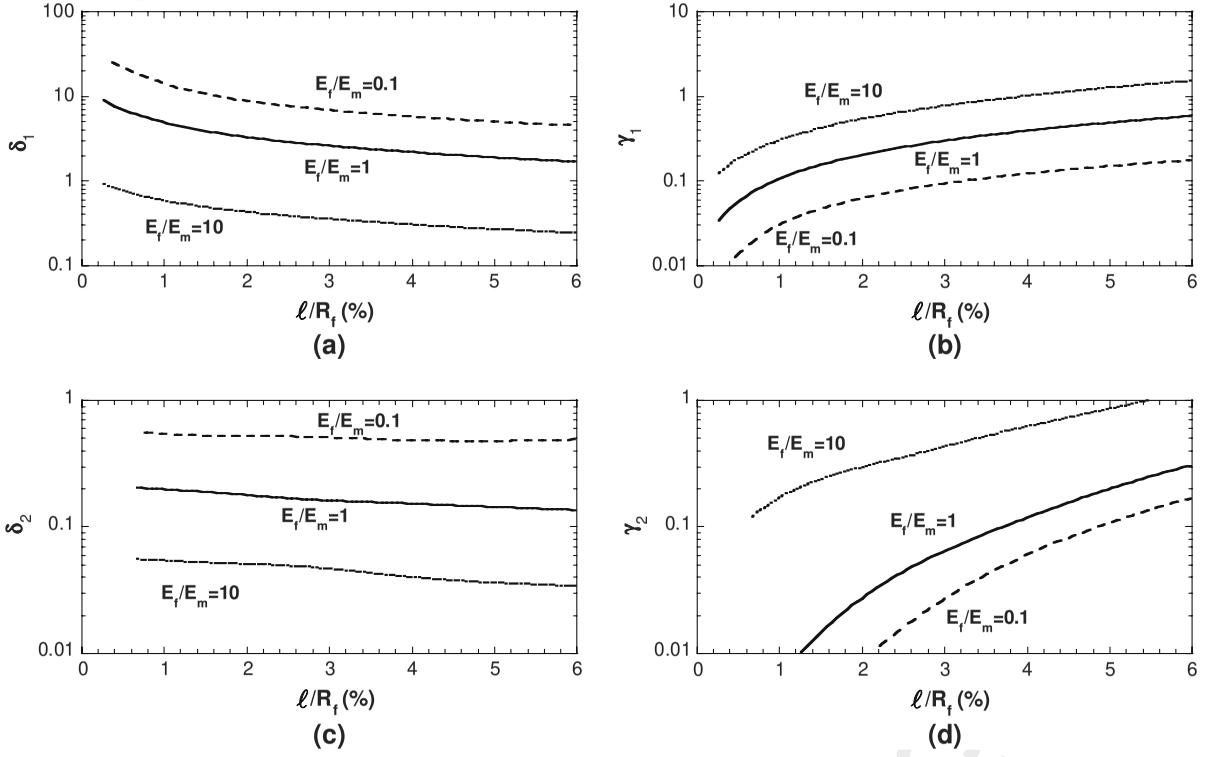

Fig. 11 Competition between fibre penetration and interfacial debonding: the structural parameters (δ_1, γ_1, δ_2, γ_2) versus the ligament width

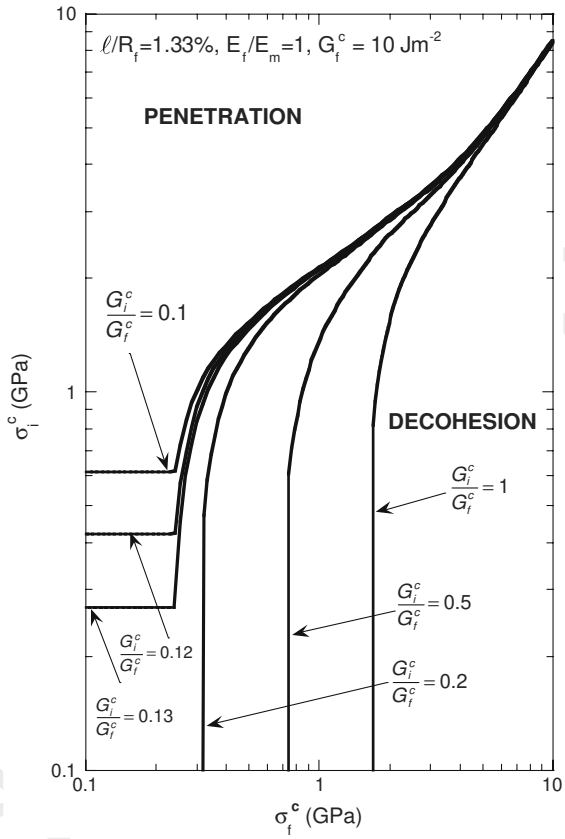

Fig. 12 Competition between fibre penetration and interfacial debonding: the penetration/debonding domain is plotted in the plane (σ_f^c, σ_i^c) for $E_f/E_m = 1$, $\ell/R_f = 1.33\%$ and $G_f^c = 10\,\mathrm{J\,m^{-2}}$

criterion for interfacial deflection for this class of materials is derived from relation (36) and combine the interfacial toughness and the fibre strength with $G_i^c < \gamma_2 \frac{R_f E_i}{E_f^2} \left(\sigma_f^c\right)^2$.

The boundaries of the decohesion domain can also be plotted in the (σ_f^c, σ_i^c) plane. Figure 12 plots this map for $E_f/E_m = 1$ and a fixed value of the ligament width. The frontiers of the domain are computed for a given value of the fibre toughness ($G_f^c = 10\,\mathrm{J\,m^{-2}}$) and various values of the interfacial toughness. This figure confirms that decohesion is facilitated by a weak value of the toughness ratio G_i^c/G_f^c. In the case of low values of the characteristic fracture lengthes L_i^c and L_f^c, both mechanisms tend to be controlled by the stress conditions (12) and (21) so that the decohesion criterion (33) leads to

$$\sigma_i^c < \left[\frac{E_i}{E_f}\frac{k_{rr}(\ell,0)}{k_{zz}(\ell,0)}\right]\sigma_f^c = S_{dp}(\ell)\sigma_f^c \tag{39}$$

which is the upper limit obtained in Fig. 12 for higher values of (σ_f^c, σ_i^c). For larger values of the characteristic fracture lengths L_i^c and L_f^c (and thus smaller values of σ_i^c and σ_f^c), strength thresholds are now observed depending on the value of the $\frac{G_i^c}{G_f^c}$ ratio.

5 Conclusion

The ability of an interface to deflect a crack must be understood in order to improve the damage tolerance of composites and laminated materials. While previous studies in the literature considered a main crack impinging on the interface, the present work analyses the initiation of interfacial debonding and fibre cracking ahead of a matrix crack tip. The analysis was conducted in the case of a cracked axisymmetric fibre/matrix cell submitted to a monotonic tensile loading. A fracture criterion based on energy and stress conditions was used in order to determine the influence of strength and toughness of the interface and fibre on the crack deflection mechanism. This "finite fracture mechanics" approach allows estimating the applied strain and the nucleation length at initiation without invoking a pre-existing kink.

For each mechanism (interface debonding and fibre cracking), the comparison between a characteristic fracture length $L^c = EG^c/(\sigma^c)^2$ and a structural parameter $L^{\max}$ allows to distinguish a large characteristic fracture length ($L^c \geq L^{\max}$) from a small one ($L^c < L^{\max}$). In the first case, the initiation length is a structural parameter and the applied strain at initiation does not depend on the strength. In the second one, the nucleation length and the applied strain at initiation both depend on the geometry and the two fracture parameters (σ^c, G^c).

The analysis of the competition between matrix cracking and the fracture mechanisms shows that the penetration criterion (respectively the debonding criterion) can only be reduced to an energy condition $G_f^c/G_m^c < W_{pm}$ (respectively $G_i^c/G_m^c < W_{dm}$) if the fibre characteristic length (respectively the interfacial characteristic length) is large enough with $L_f^c \geq L_p^{\max}$ (respectively $L_i^c \geq L_d^{\max}$). Exploring the domain of small characteristic fracture lengths reveals strength thresholds ($\sigma_p^{th}, \sigma_d^{th}$) which allow to protect the fibre from crack penetration (with the condition $\sigma_f^c > \sigma_p^{th}$) or to promote interfacial decohesion (with the condition $\sigma_i^c < \sigma_d^{th}$). Those strength thresholds are depending on the matrix toughness and the geometry.

The analysis of the competition between fibre cracking and interfacial debonding is more complex because all the fracture parameters ($G_f^c, \sigma_f^c, G_i^c, \sigma_i^c$) are involved. Comparing the characteristic fracture lengths allows to assess the dominant condition for each mechanism in order to obtain a simple condition for debonding:

(i) large values of the fracture lengths ($L_i^c \geq L_d^{\max}, L_f^c \geq L_p^{\max}$) lead to the energy criterion $G_i^c/G_f^c < W_{dp}$,
(ii) small values of the fracture lengths ($L_i^c \to 0, L_f^c \to 0$) lead to the stress criterion $G_i^c/G_f^c < S_{dp}$.

The introduction of the structural parameters (δ_1, δ_2) allows to define a "strong" or a "weak" interface with $\sigma_i^c/\sigma_f^c \geq \delta_1$ or $\sigma_i^c/\sigma_f^c \leq \delta_2$. In the first case, fibre penetration is predicted if

$$G_f^c < \gamma_1 \frac{R_f E_f}{E_i^2} (\sigma_i^c)^2$$

(whatever the value of the interfacial toughness G_i^c) while in the second one interfacial debonding requires

$$G_i^c < \gamma_2 \frac{R_f E_i}{E_f^2} \left(\sigma_f^c\right)^2$$

(whatever the value of the fibre toughness G_f^c). Those results show that the criterion for interfacial deflection can combine strength and toughness as already pointed out by the recent work of (Parmigiani and Thouless 2006). These authors consider a different situation with the

matrix crack tip located at the bimaterial interface and use cohesive zone models to analyse the competition between deflection and penetration. Cohesive zone models are an alternative to fracture criteria and it is to be noted that a recent asymptotic analysis has demonstrated an excellent agreement between the stress-energy criterion and the Dugdale cohesive zone model to predict the initiation of failure at a V-notch in brittle elastic materials under mode I loading (Henninger et al. 2007).

Acknowledgements Part of this work was carried out under the AMERICO project (Multiscale Analyses: Innovating Research for Composites) directed by ONERA (French Aeronautics and Space Research Centre). The authors would like to acknowledge support from DGA/STTC (French Ministry of Defence).

Appendix. Finite element analysis

Due to symmetry in the geometry and the boundary conditions, the elastic finite element calculations are only performed on a quarter of the single fibre composite cylinder as shown in Fig. 2b. Linear axisymmetric elements are used throughout the analysis. Very fine meshes are used to limit inaccuracy. The size of the smallest element which is immediately adjacent to the crack tip is chosen to be less than $\ell/50$. Half the length L of the unit cell is chosen as $L = 10R_f$. This value is selected to simulate a structure with an infinite length by comparing the far field stress given by the finite element solution with the classical Lamé solution for a damage free concentric cylinder model (Mc Cartney 1989). The resulting mesh typically contains a number of nodes varying from 10,000 to 30,000. The energy release rate is computed with the help of a virtual crack closure integral method. This local energy method was shown to provide good results if the layout of the mesh around the crack tip is homogeneous (Buchholz et al. 1999). The adequacy of the mesh refinement was evaluated by performing a convergence study and comparing with the results of (Liu et al. 1997) who consider the problem of a matrix crack approaching an interface by solving singular integral equations. The finite element library Modulef is used as the analysis tool (Bernadou et al. 1988).

References

Bernadou M et al (1988) MODULEF: a finite element library. INRIA, Roquencourt, France

Buchholz FG, Chergui A, Richard HA (1999) Computational fracture analysis by means of virtual crack closure integrals. In: Garcia Garino C, Mirasso A, Baron J, Nunez McLeod J (eds) Mecanica computational. Mecom99, Mendoza

Domergue JM, Vagaggini E, Evans AG (1995) Relationships between hysteresis measurements and the constituent properties of ceramic matrix composites II: experimental studies on unidirectional materials. J Am Ceram Soc 95:2721–2731. doi:10.1111/j.1151-2916.1995.tb08047.x

Evans AG, Zok FW, Davis JB (1991) The role of the interface in fiber reinforced brittle matrix. Compos Sci Technol 42:3–24. doi:10.1016/0266-3538(91)90010-M

He MY, Hutchinson JW (1989) Crack deflection at an interface between dissimilar elastic materials. Int J Solids Struct 25:1053–1067. doi:10.1016/0020-7683(89)90021-8

Henninger C, Leguillon D, Martin E (2007) Crack initiation at a V-notch – comparison between a brittle fracture criterion and the Dugdale cohesive model. C R Mecanique 335:388–393

Hutchinson JW, Mear ME, Rice JR (1987) Crack paralleling an interface between dissimilar materials. ASME J Appl Mech 54:828–832

Kagawa Y, Goto K (1998) Direct observation and modelling of the crack fibre interaction process in continuous fibre-reinforced ceramics: model experiments. Mater Sci Eng A 250:285–290. doi:10.1016/S0921-5093(98)00603-0

Kerans RJ, Hay RS, Parthasarathy TA, Cinilbulk MK (2002) Interface design for oxydation-resistant ceramic composite. J Am Ceram Soc 85:2599–2632

Lee W, Howard SJ, Clegg WJ (1996) Growth of interface defects and its effect on crack deflection and toughening criteria. Acta Mater 44:3905–3922. doi:10.1016/S1359-6454(96)00068-7

Leguillon D (2002) Strength or toughness? A criterion for crack onset at a notch. Eur J Mech A/Solids 21:61–72

Leguillon D, Sanchez-Palencia E (1992) Fracture in heterogeneous materials: weak and strong singularities. In: Ladeveze P, Zienkiewicz OC (eds) New advances in computational structural mechanics, studies in applied mathematics, vol 32. Elsevier, Amsterdam, pp 423–434

Leguillon D, Yosibash Z (2003) Crack onset at a V-Notch. Influence of the notch tip radius. Int J Fract 122:1–21. doi:10.1023/B:FRAC.0000005372.68959.1d

Leguillon D, Lacroix C, Martin E (2000) Interface debonding ahead of a primary crack. J Mech Phys Solids 48:2137–2161. doi:10.1016/S0022-5096(99)00101-5

Liu YF, Tanaka Y, Masuda C (1997) Analysis of the fiber-matrix cylindrical model with a circumferential crack. Int J Fract 88:87–105. doi:10.1023/A:1007463422102

Majumdar BS, Gundel DB, Dutton RE, Warrier SG, Pagano NJ (1998) Evaluation of the tensile interface strength in brittle matrix composite systems. J Am Ceram Soc 81:1600–1610

Martinez D, Gupta V (1994) Energy criterion for crack deflection at an interface between two orthotropic media. J Mech Phys Solids 42:1247–1271. doi:10.1016/0022-5096(94)90034-5

Martin E, Leguillon D (2004) Energetic conditions for interfacial failure in the vicinity of a matrix crack in brittle matrix composites. Int J Solids Struct 41:6937–6948. doi:10.1016/j.ijsolstr.2004.05.044

Martin E, Leguillon D, Lacroix C (2001) A revisited criterion for crack deflection at an interface in brittle matrix composites. Compos Sci Technol 61:1671–1679. doi:10.1016/S0266-3538(01)00067-7

Martin E, Leguillon D, Lacroix C (2002) An energy criterion for the initiation of interfacial failure ahead of a matrix crack in brittle matrix composites. Compos Interf 9:143–156. doi:10.1163/156855402760116076

Mc Cartney LN (1989) New theoretical model of stress transfer between fibre and matrix in a uniaxially fibre-reinforced composite. Proc R Soc Lond A Math Phys Sci 425:215–244. doi:10.1098/rspa.1989.0104

Mc Clintock FA (1958) Ductile fracture instability in shear. J Appl Mech 25:582–588

Muller A, Becker W, Stolten D, Hohe J (2006) A hybrid method to assess interface debonding by finite fracture mechanics. Eng Fract Mech 73:994–1008. doi:10.1016/j.engfracmech.2005.12.001

Nairn JA (2001) Fracture mechanics of composites with residual stresses,imperfect interfaces, and traction-loaded cracks. Compos Sci Technol 61:2159–2167. doi:10.1016/S0266-3538(01)00110-5

Novozhilov V (1969) On a necessary and sufficient criterion for brittle strength. J Appl Math Mech (translation of PMM) 33:212–222

Pagano NJ (1998) On the micromechanical failure modes in a class of ideal brittle matrix composites, part 1. Coated-fiber composites. Compos B 29B:93–119. doi:10.1016/S1359-8368(97)00002-4

Parmigiani JP, Thouless MD (2006) The roles of thoughness and cohesive strength on crack deflection at interfaces. J Mech Phys Solids 54:266–287. doi:10.1016/j.jmps.2005.09.002

Phillipps AJ, Clegg WJ, Clyne TW (1994) The failure of layered ceramics in bending and tension. Composites 25:524–533. doi:10.1016/0010-4361(94)90180-5

Pronin AN, Gupta V (1998) Measurement of thin film interface toughness by using laser-generated stress pulses. J Mech Phys Solids 46:389–410. doi:10.1016/S0022-5096(97)00081-1

Seweryn A (1994) Brittle fracture criterion for structures with sharp notches. Eng Fract Mech 47:673–681. doi:10.1016/0013-7944(94)90158-9

Whitney JM, Huismer RJS (1974) Stress fracture criteria for laminated composites containing stress concentrations. J Comp Mater 8:71–108. doi:10.1177/002199837400800303

Xu LR, Huang YY, Rosakis AJ (2003) Dynamic crack deflection and penetration at interfaces in homogeneous materials: experimental studies and model predictions. J Mech Phys Solids 51:461–486. doi:10.1016/S0022-5096(03)00067-X